Int. J. Appl. Math. Comput. Sci., 2018, Vol. 28, No. 4, 679–693
DOI: 10.2478/amcs-2018-0052

amcs

ADAPTIVE BACKSTEPPING TRACKING CONTROL FOR AN OVER–ACTUATED DP MARINE VESSEL WITH INERTIA UNCERTAINTIES

ANNA WITKOWSKA [a,*], ROMAN ŚMIERZCHALSKI [a]

[a]Faculty of Electrical and Control Engineering
Gdańsk University of Technology, G. Narutowicza 11/12, 80-233 Gdańsk, Poland
e-mail: anna.witkowska@pg.edu.pl

Designing a tracking control system for an over-actuated dynamic positioning marine vessel in the case of insufficient information on environmental disturbances, hydrodynamic damping, Coriolis forces and vessel inertia characteristics is considered. The designed adaptive MIMO backstepping control law with control allocation is based on Lyapunov control theory for cascaded systems to guarantee stabilization of the marine vessel position and heading. Forces and torque computed from the adaptive control law are allocated to individual thrusters by employing the quadratic programming method in combination with the cascaded generalized inverse algorithm, the weighted least squares algorithm and the minimal least squares algorithm. The effectiveness of the proposed control scheme is demonstrated by simulations involving a redundant set of actuators. The evaluation criteria include energy consumption, robustness, as well accuracy of tracking during typical vessel operation.

Keywords: over-actuated control, adaptive control, Lyapunov function, control allocation, MIMO system.

1. Introduction

Dynamic positioning systems (DPSs) were first used in the offshore industry to automatically maintain the position and heading of ships at low speed in the presence of disturbances. This task is realized through independent control in three degrees of freedom (DOFs), by using only own thrusters and propellers to generate forces and torques in various directions. The currently designed DPSs are multi-task systems. They perform additional operations such as dynamic mooring, automatic station keeping and trajectory tracking. For station keeping applications, nonlinear damping as well Coriolis and centripetal forces can be neglected, while only the nonlinearity in ship kinematics is considered. Tracking the operation of a marine vessel at a low speed refers to simultaneous control of the surge and sway position as well as the yaw angle. In this case, the kinematic and dynamic equations of motion include nonlinearities that are mostly unpredictable due to changes in operating points and the influence of environmental disturbances. This motivates the application of the adaptive, nonlinear control theory for designing a dynamic positioning (DP) control law. Furthermore, in modern DP vessels the type of over-actuated control takes place when the total number of control inputs exceeds the total number of controlled degrees of freedom. In this case the commanded forces and torque in 3 DOFs have to be divided into particular command settings for actuators by the control allocation (CA) unit, taking into account physical constraints of actuators demands.

The DP controller and CA can be analyzed separately based on the separation principle (Loria *et al.*, 2000) and the interconnection between them. A survey of selected major research works and technology advances in DP controller design is presented by Sorensen (2011). Conventional ship control systems are designed under the assumption that kinematic and dynamic equations of motion can be linearized at their nominal operating points by using linear multi-controllers (Bańka *et al.*, 2013) or Kalman filtering methods (Fossen *et al.*, 1996). For dynamic positioning purposes, the nonlinear model-based position and heading control algorithms make use of LQG, sliding mode control (Tannuri *et al.*, 2010), robust H_∞ control (Katebi *et al.*, 1997), dynamic

*Corresponding author

surface control (DSC) (Swaroop *et al.*, 2000), active direct surface control (Fu *et al.*, 2016) and more advanced hybrid switching control techniques (Tomera, 2017). The use of artificial intelligence (McGookin *et al.*, 2000), fuzzy logic and neural nets for DP control systems is also presented in the literature. Robust low speed controllers for different sea conditions (calm, moderate, high and extreme seas) are developed based on a linear model with parametric uncertainties by using H_∞ and mixed-μ techniques (Hassani *et al.*, 2012).

Control allocation algorithms for DPSs differ by the definition of the objective function and the optimization methods used. Real DP control systems reveal a limited potential of data processing, with simultaneous high requirements concerning software reliability. That is why many practical solutions make use of simple optimisation algorithms and base on their effective implementation (Lindegaard and Fossen, 2003). A detailed overview of existing methods is provided by Johansen and Fossen (2013).

A majority of present solutions consist in calculating a pseudoinverse matrix and the use of classical optimization methods, such as methods of Lagrange multipliers or the least squares. They usually assume a square objective function which minimizes the activity of actuators. A large number of optimisation methods take into account constraints connected with saturation of actuators. Here, the penalty function method (Bodson, 2002), the direct allocation (DA) method, the redistributed pseudoinverse solution (RPI) method (Oppenheimer *et al.*, 2006) and cascaded methods of generalized inverse solutions (CGI cascaded generalized inverse) can be named. In many works the control allocation problem is viewed as a static or quasi-dynamic optimization one that is solved independently of the dynamic control problem considering non-adaptive linear effector models and neglecting actuator dynamics. The model predictive control allocation (MPCA) algorithm taking into account the information on the model of the dynamics of actuators described by a linear time-varying actuator model for calculating control signal settings is proposed for vehicles by Luo *et al.* (2004) and Hanger *et al.* (2011). There are several approaches of an adaptive control allocation in the case of actuator failures which are tested via simulation (Witkowska and Śmierzchalski, 2018).

The backstepping method is a widely applied nonlinear control technique for dynamic positioning of over-actuated marine vessels, such as ships (Fossen, 2000; Witkowska, 2013; Lin *et al.*, 2013; Zhang *et al.*, 2013; Zwierzewicz, 2010) or platforms (Tsopelakos and Papadopoulos, 2017). The uncertain ship dynamics and environmental disturbances were also compensated by systems being a combination of the backstepping method with fuzzy logic (Xia *et al.*, 2016) or RBF neural networks (Du *et al.*, 2015; Boulkroune *et al.*, 2014) used for approximation of stability functions. In comparison with other methodologies, the vectorial nonlinear backstepping method is effective in dynamic positioning but computationally very complex. Among other reasons, this complexity results from the need for analytical calculation of stability functions and overparametrization (Krstić *et al.*, 1995; Witkowska and Śmierzchalski, 2012) that may result in a significant increase in the number of tuning functions and design parameters. In the literature, only damping matrix uncertainties were considered in ship models, while the inertia and Coriolis matrices were neglected in backstepping design. In some applications, such as ship-to-ship (STS) transfer operations, the carrying of non-homogeneous loads, a loss of cargo or a leakage, the parameters of the inertia matrix will also vary. In this case, it is necessary to estimate the current ship mass for ship stability requirements.

This paper studies Lyapunov stability theory-based design of the adaptive backstepping control law for an MIMO multivariable over-actuated DP ship with an unknown matrix system. The uncertainties in the DPS are related completely unknown ship dynamic model parameters as well slowly varying environmental disturbances. The paper gives a precise description of the method to determine the regression matrix for the analyzed system, which is a very difficult problem. The regression matrix is determined indirectly in the ship dynamics model, but only at the stage of creating the Lyapunov function, which significantly simplifies the standard procedure of the backstepping control law design. By means of the LaSalle invariant theorem and Lyapunov control function theory, the output feedback guarantees that all signals in the closed-loop DP control system are uniformly ultimately bounded. The forces and torque computed from the adaptive control law are allocated to individual thrusters by employing quadratic programming (QP). A comparison between the cascaded generalized inverse (CGI) algorithm, the weighted least squares (WLS) algorithm and the minimal least squares (MLS) algorithm is made. The effectiveness of the proposed control scheme is demonstrated by simulations involving a redundant set of actuators. The evaluation criteria include energy consumption represented by the square norm of control inputs, robustness and accuracy of dynamic positioning during typical vessel operations.

2. System description and problem formulation

The analyzed mathematical model of a DP marine vessel (plant) consists of vessel dynamics with environmental disturbances, kinematics, force generation and actuator dynamics as subsystems in a cascaded structure.

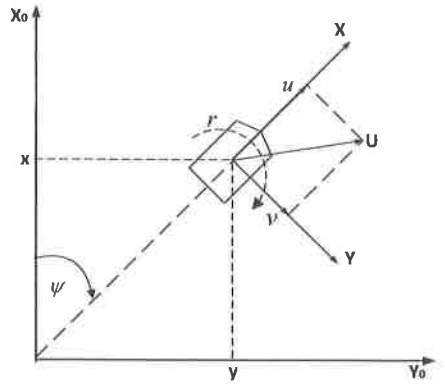

Fig. 1. Earth-fixed and body-fixed coordinate frames.

2.1. Ship dynamics and kinematics. For DP marine vessel tracking applications, it is convenient to consider nonlinearities in the dynamic and kinematic models in the horizontal plane (Fossen, 2011). The equations of ship motion,

$$\dot{\boldsymbol{\eta}} = \mathbf{J}(\boldsymbol{\eta})\,\mathbf{v}, \tag{1}$$

$$\mathbf{M}\dot{\mathbf{v}} + \mathbf{C}(\mathbf{v})\mathbf{v} + \mathbf{D}(\mathbf{v})\,\mathbf{v} = \boldsymbol{\tau} + \boldsymbol{\tau}_{\text{env}}, \tag{2}$$

are developed using the Earth-fixed frame X_0Y_0 with the origin taken at an arbitrary point on the Earth's surface and the body-fixed frame XY with the origin taken at the center of gravity of the ship (Fig. 1). The output vector $\boldsymbol{\eta} = [x, y, \psi]^T \in \mathbb{R}^3$ of the system (1)–(2) consists of the ship's position (x, y) and heading $\psi \in [0, 2\pi]$ in the Earth-fixed frame. Vector $\mathbf{v} = [u, v, r]^T \in \mathbb{R}^3$ includes the ship's surge, sway and yaw velocities, respectively, in the body fixed frame. The input vector $\boldsymbol{\tau} = [\tau_x, \tau_y, \tau_n]^T \in \mathbb{R}^3$ represents the forces and torque coming from the thrusters and propulsion devices (actuators) in the body-fixed frame. The vector $\boldsymbol{\tau}_{\text{env}} \in \mathbb{R}^3$ describes, in the Earth-fixed frame, the unmodeled dynamics and environmental disturbances, which come from wind, waves and currents. Other terms are as follows:

$$\mathbf{J}(\boldsymbol{\eta}) = \begin{bmatrix} \cos\psi & -\sin\psi & 0 \\ \sin\psi & \cos\psi & 0 \\ 0 & 0 & 1 \end{bmatrix} \in \mathbb{R}^{3\times 3},$$

the state-dependent transformation matrix from the vessel-fixed to the Earth-fixed frame;

$$\mathbf{M} = \begin{bmatrix} m_{11} & 0 & 0 \\ 0 & m_{22} & m_{23} \\ 0 & m_{32} & m_{33} \end{bmatrix} \in \mathbb{R}^{3\times 3},$$

the inertia matrix;

$$\mathbf{D} = \begin{bmatrix} d_{11}(\mathbf{v}) & 0 & 0 \\ 0 & d_{22}(\mathbf{v}) & d_{23}(\mathbf{v}) \\ 0 & d_{32}(\mathbf{v}) & d_{33}(\mathbf{v}) \end{bmatrix} \in \mathbb{R}^{3\times 3},$$

the damping matrix;

$$\mathbf{C} = \begin{bmatrix} 0 & 0 & c_{13}(\mathbf{v}) \\ 0 & 0 & c_{23}(\mathbf{v}) \\ -c_{13}(\mathbf{v}) & -c_{23}(\mathbf{v}) & 0 \end{bmatrix} \in \mathbb{R}^{3\times 3},$$

the skew-symmetric Coriolis and centripetal matrix.

Here $\mathbf{M} = \{m_{ij}\}$ is defined as $m_{11} = m - X_{\dot{u}}$, $m_{22} = m - Y_{\dot{v}}$, $m_{23} = mx_G - Y_{\dot{r}}$, $m_{32} = mx_G - N_{\dot{v}}$, $m_{33} = I_z - N_{\dot{r}}$ related to the added mass terms, as well as the vessel mass m and moment of inertia I_z about the body-fixed Z-axis, while x_G is the distance between the center of gravity and the origin of the body-fixed frame; $\mathbf{D} = \{d_{ij}\}$ is defined as $d_{11} = -X_u - X_{|u|u}|u|$, $d_{22} = -Y_v - Y_{|v|v}|v| - Y_{|r|v}|r|$, $d_{23} = -Y_r - Y_{|v|r}|v| - Y_{|r|r}|r|$, $d_{32} = -N_v - N_{|v|v}|v| - N_{|r|v}|r|$, $d_{33} = -N_r - N_{|v|r}|v| - N_{|r|r}|r|$ with terms related to hydrodynamic damping forces during vessel movement on water; $\mathbf{C} = \{c_{ij}\}$ is defined as $c_{13} = -(m - Y_{\dot{v}})v - (mx_G - Y_{\dot{r}})r$, $c_{23} = (m - X_{\dot{u}})u$.

The vector $\boldsymbol{\tau}_{\text{env}}$ generally describes high and low frequency forces and moments acting on the vessel. The low frequency part, driven by loads generated by a second-order mean and slowly varying wave, current and wind, has to be counteracted by the control inputs. The high-frequency part has to be filtered from the measurements by using a Kalman filter, a particle Kalman filter, a backstepping observer or a passive observer. In the paper only the low-frequency part of $\boldsymbol{\tau}_{\text{env}}$ is considered assuming that one of the filtering techniques has been successfully implemented. The influence of the unmodeled part of slowly varying disturbances is taken into account as an additional force acting on the ship $\boldsymbol{\tau}_{\text{env}} = \mathbf{J}^T(\boldsymbol{\eta})\mathbf{b}$, where the bias term $\mathbf{b} = [b_1, b_2, b_3]^T \in \mathbb{R}^{3\times 1}$ is modeled by

$$\dot{\mathbf{b}} = -\mathbf{F}^{-1}\mathbf{b} + \mathbf{E}\mathbf{w} \tag{3}$$

as the first-order Markov process. This model (3) includes time constants $\mathbf{F} = \text{diag}(1000, 1000, 1000)$ and the gain matrix $\mathbf{E} = \text{diag}(3000, 3000, 30000)$ (Du *et al.*, 2015) of zero-mean white noise vector $\mathbf{w} \in \mathbb{R}^{3\times 1}$.

2.2. Force generation and actuator dynamics. The thruster model

$$\boldsymbol{\tau} = \mathbf{B}(\beta)\,\mathbf{f}, \tag{4}$$
$$\mathbf{f} = \mathbf{K}(\mathbf{v})\mathbf{u},$$

describes the relation between the thrust forces $\mathbf{f} \in \mathbb{R}^{r\times 1}$ and moment $\boldsymbol{\tau}$ acting on the vessel and the vector of actuator states $\mathbf{u}$. The thrust forces $\mathbf{f}$ are distributed to the surge, sway and yaw directions by the actuator configuration matrix $\mathbf{B} \in \mathbb{R}^{3\times r}$, depending on the location of the actuators and on the vector of thrust angles β (in the case of rotatable thrusters). The matrix $\mathbf{K} \in \mathbb{R}^{r\times r}$ is a diagonal thrust efficiency coefficient matrix (control effectiveness matrix) dependent on the ship's velocity, density of water, the propeller's diameter and revolutions, and the type of actuators. The input vector $\mathbf{u} \in \mathbb{R}^{r\times 1}$ of the subsystem (4) describes the constrained actuator states, where $r \geq 3$ is the total number of control inputs. The dynamics of each individual actuator

$$\mathbf{T}\dot{\mathbf{u}} + \mathbf{u} = \mathbf{u}_c \tag{5}$$

are defined in dependence on the diagonal matrix $\mathbf{T} \in \mathbb{R}^{r\times r}$ of actuator time constants and the input vector $\mathbf{u}_c \in \mathbb{R}^{r\times 1}$, which represents the commanded actuator states.

The purpose of the study is to develop a control law capable of performing a basic task in ship dynamic positioning, which is tracking the reference signal $\boldsymbol{\eta}_d = [x_d, y_d, \psi_d]^T$ of the position and heading at a low speed with completely unknown ship dynamics (1)–(2) and slowly varying environmental disturbances, with the main attention focused on inertia matrix uncertainties. The backstepping methodology used for nonautonomous systems ensures asymptotic convergence to reference values, while all signals in the DP closed loop control system are globally uniformly ultimately bounded. To fulfil this control objective, it is assumed that the real ship position and heading can be controlled independently in 3 DOFs.

2.3. State-space representation. The tracking problem will be considered for the continuous plant model without actuator dynamics (1)–(4). It can be expressed in the state-space representation

$$\dot{\boldsymbol{\eta}} = \mathbf{J}(\boldsymbol{\eta})\,\mathbf{v}, \tag{6}$$

$$\mathbf{M}\dot{\mathbf{v}} = \boldsymbol{\theta}\hat{\mathbf{u}} + \boldsymbol{\varphi}_1^T(\boldsymbol{\eta}, \mathbf{v})\,\boldsymbol{\theta}_1, \tag{7}$$

where

$$\boldsymbol{\theta}\hat{\mathbf{u}} \in \mathbb{R}^{3\times 1}, \quad \boldsymbol{\theta} = \mathbf{BK} \in \mathbb{R}^{3\times r},$$

$$\boldsymbol{\varphi}_1^T(\boldsymbol{\eta}, \mathbf{v})\,\boldsymbol{\theta}_1 = -\mathbf{D}\mathbf{v} - \mathbf{C}\mathbf{v} + \mathbf{J}^T(\boldsymbol{\eta})\,\mathbf{b} \in \mathbb{R}^{3\times 1}, \boldsymbol{\theta}_1,$$

$$\begin{aligned}\boldsymbol{\theta}_1 = [&X_u, Y_v, Y_r, N_v, N_r, X_{|u|u}\\ &Y_{|v|v}, Y_{|r|v}, Y_{|v|r}, Y_{|r|r},\\ &N_{|v|v}, N_{|r|v}, N_{|v|r}, N_{|r|r},\\ &m - Y_{\dot{v}},\ mx_G - Y_{\dot{r}}, -(m - X_{\dot{u}}),\\ &b_1, b_2, b_3]^T \in \mathbb{R}^{20\times 1},\end{aligned}$$

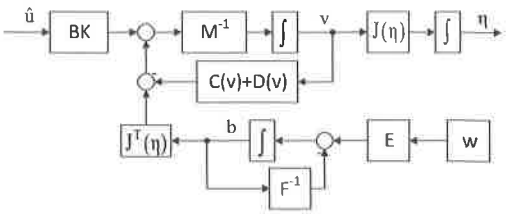

Fig. 2. Block diagram of the ship model.

$$\boldsymbol{\varphi}_1^T = [\mathbf{A_C}\ \mathbf{A_D}\ \mathbf{A_J}] \in \mathbb{R}^{3\times 20},$$

$$\mathbf{A}_C = \begin{bmatrix} u & 0 & 0 & 0 & 0 & |u|\,u & 0 & 0\\ 0 & v & r & 0 & 0 & 0 & |v|\,v & |r|\,v\\ 0 & 0 & 0 & v & r & 0 & 0 & 0\\ 0 & 0 & & & & & & \\ |v|\,r & |r|\,r & & & & & & \\ 0 & 0 & & & & & & \end{bmatrix},$$

$$\mathbf{A_D} = \begin{bmatrix} 0 & 0 & 0 & 0\\ 0 & 0 & 0 & 0\\ |v|\,v & |r|\,v & |v|\,r & |r|\,r \end{bmatrix},$$

$$\mathbf{A_J} = \begin{bmatrix} vr & r^2 & 0 & \cos\psi & \sin\psi & 0\\ 0 & 0 & ur & -\sin\psi & \cos\psi & 0\\ -vu & -ru & -uv & 0 & 0 & 1 \end{bmatrix}.$$

The block diagram of the state-space model is presented in Fig. 2. The ship actuator dynamics (5) are neglected in the design process. In this case, $\boldsymbol{\eta}$, $\mathbf{v}$ are the states, while $\hat{\mathbf{u}}$ represents the control input vector to the plant.

The nonlinear matrix system (3)–(7) satisfies the following properties.

Assumption 1.

1. $\mathbf{M}^T = \mathbf{M} \Rightarrow \mathbf{x}^T\mathbf{M}\mathbf{x} > 0,\ \mathbf{x} \neq 0.$

2. $\mathbf{J}^{-1}(\boldsymbol{\eta}) = \mathbf{J}^T(\boldsymbol{\eta}),\ \|\mathbf{J}(\boldsymbol{\eta})\| = 1.$

3. $\dfrac{\mathrm{d}}{\mathrm{d}t}\mathbf{J}^T(\boldsymbol{\eta}) = -r\mathbf{S}\mathbf{J}^T(\boldsymbol{\eta})$, where

$$\mathbf{S} = \begin{bmatrix} 0 & -1 & 0\\ 1 & 0 & 0\\ 0 & 0 & 0 \end{bmatrix}, \quad \mathbf{S} = -\mathbf{S}^T.$$

4. $\boldsymbol{\theta}$ is regular, so there exists a pseudoinverse matrix $\boldsymbol{\theta}^+$ satisfying $\boldsymbol{\theta}^+\boldsymbol{\theta} = \mathrm{I}$.

The following assumption can be made when designing the control law.

Assumption 2.

1. The parameters of matrices $\mathbf{D}, \mathbf{C}, \mathbf{M}$ are unknown and slowly varying.
2. All states are available for feedback and bounded. The vessel position and heading are measured and filtered, the nonmeasured velocity vector is estimated and they coincide with the real values.
3. State reference trajectories $\boldsymbol{\eta}_{\mathrm{d}}$ as well their first-and second-order derivatives $\dot{\boldsymbol{\eta}}_{\mathrm{d}}$, $\ddot{\boldsymbol{\eta}}_{\mathrm{d}}$ are smooth and bounded.
4. Slowly varying environmental disturbances $\mathbf{b}$ are unknown.

3. MIMO backstepping tracking and stability analysis

The MIMO vectorial backstepping methodology, discussed in detail by Fossen (2011), is used to design the DP control law. The design process consists of two stages, focused on designing kinematic and dynamic controllers. At the kinematic level (6), the control objective is to adjust the position $\boldsymbol{\eta}(t)$ to the desired value $\boldsymbol{\eta}_{\mathrm{d}}(t), t \geq 0$. At this stage the vector $\mathbf{v}(t)$ is taken as a virtual control input with the corresponding virtual control laws $\boldsymbol{\alpha}(t) = [\alpha_1, \alpha_2, \alpha_3]^T \in \mathbb{R}^{3\times 1}$ calculated with respect to the first control Lyapunov function candidate (CLF). At the dynamic level (7), the control objective is to stabilize the system with uncertainties at $\mathbf{v}(t) \approx \mathbf{0}$. At this stage, the commanded virtual vector of forces and torque is designed based on the second CLF, complemented by the function of unknown parameters. The allocation of the commanded forces and torque to the commanded actuator states $\widehat{\mathbf{u}}(t)$ is calculated by the control allocation algorithm based on quadratic programming.

3.1. DP controller. Following the backstepping methodology, the system is considered in new state variables $\mathbf{z}_1(t) \in \mathbb{R}^{3\times 1}$ and $\mathbf{z}_2(t) \in \mathbb{R}^{3\times 1}$, which are defined as the error vectors

$$\mathbf{z}_1 = \mathbf{J}^T(\boldsymbol{\eta})(\boldsymbol{\eta} - \boldsymbol{\eta}_{\mathrm{d}}), \tag{8}$$

$$\mathbf{z}_2 = \mathbf{v} - \boldsymbol{\alpha} \tag{9}$$

in the body-fixed coordinate system, respectively for the kinematics (8) and the dynamics (9). The time derivative of the first state variable

$$\dot{\mathbf{z}}_1 = -r\mathbf{S}\mathbf{z}_1 + \mathbf{v} - \mathbf{J}^T(\boldsymbol{\eta})\dot{\boldsymbol{\eta}}_{\mathrm{d}} \tag{10}$$

is first calculated based on Eqns. (8) and (6), and Assumptions 1.2–1.3. Then, after adopting the assumption (9), it takes the form

$$\dot{\mathbf{z}}_1 = -r\mathbf{S}\mathbf{z}_1 + \mathbf{z}_2 + \boldsymbol{\alpha} - \mathbf{J}^T(\boldsymbol{\eta})\dot{\boldsymbol{\eta}}_{\mathrm{d}}. \tag{11}$$

The time derivative of the second state variable

$$\dot{\mathbf{z}}_2 = \dot{\mathbf{v}} - \dot{\boldsymbol{\alpha}} = \mathbf{M}^{-1}(\boldsymbol{\theta}\widehat{\mathbf{u}} + \boldsymbol{\varphi}_1^T\boldsymbol{\theta}_1 - \mathbf{M}\dot{\boldsymbol{\alpha}}) \tag{12}$$

is obtained in the light of (9) and (7).

Let us write the component $-\mathbf{M}\dot{\boldsymbol{\alpha}}$ in regression form $-\mathbf{M}\dot{\boldsymbol{\alpha}} = \boldsymbol{\varphi}_2^T(\boldsymbol{\eta}, \mathbf{v}, \dot{\boldsymbol{\eta}}_{\mathrm{d}}, \ddot{\boldsymbol{\eta}}_{\mathrm{d}})\boldsymbol{\theta}_2 \in \mathbb{R}^{3\times 1}$ with the regression matrix

$$\boldsymbol{\varphi}_2^T = \begin{bmatrix} -\dot{\alpha}_1 & 0 & 0 & 0 & 0 \\ 0 & -\dot{\alpha}_2 & -\dot{\alpha}_3 & 0 & 0 \\ 0 & 0 & 0 & -\dot{\alpha}_2 & -\dot{\alpha}_3 \end{bmatrix} \in \mathbb{R}^{3\times 5}$$

and the vector $\boldsymbol{\theta}_2 = [m_{11}, m_{22}, m_{23}, m_{32}, m_{33}]^T \in \mathbb{R}^{5\times 1}$ containing all unknown parameters of $\mathbf{M}$. Now the expression (12) can be represented by

$$\dot{\mathbf{z}}_2 = \mathbf{M}^{-1}\left(\boldsymbol{\theta}\widehat{\mathbf{u}} + \boldsymbol{\varphi}_1^T\boldsymbol{\theta}_1 + \boldsymbol{\varphi}_2^T\boldsymbol{\theta}_2\right). \tag{13}$$

A natural way of finding the adaptive control law for $\boldsymbol{\theta}_i$, $i = \{1, 2\}$, consists in adopting the "certainty equivalence" principle, where the uncertainty $\boldsymbol{\theta}_i$ is replaced in (13) by the sum $\widehat{\boldsymbol{\theta}}_i + \widetilde{\boldsymbol{\theta}}_i$ of the estimate and estimation errors,

$$\begin{aligned} \dot{\mathbf{z}}_2 = \mathbf{M}^{-1}&\left(\boldsymbol{\theta}\widehat{\mathbf{u}} + \boldsymbol{\varphi}_1^T\widehat{\boldsymbol{\theta}}_1 + \boldsymbol{\varphi}_2^T\widehat{\boldsymbol{\theta}}_2\right) \\ &+ \mathbf{M}^{-1}\left(\boldsymbol{\varphi}_1^T\widetilde{\boldsymbol{\theta}}_1 + \boldsymbol{\varphi}_2^T\widetilde{\boldsymbol{\theta}}_2\right). \end{aligned} \tag{14}$$

The positive definite (Assumption 1.1) control Lyapunov function (CLF) candidate

$$\mathbf{V}_a = \frac{1}{2}\mathbf{z}_1^T\mathbf{z}_1 + \frac{1}{2}\mathbf{z}_2^T\mathbf{M}\mathbf{z}_2 + \mathbf{V}_{\mathrm{phi}} \tag{15}$$

for the entire system is considered as the weighted sum of output errors $\mathbf{z}_i$ augmented by $\mathbf{V}_{\mathrm{phi}} = \widetilde{\boldsymbol{\theta}}_1^T\boldsymbol{\Gamma}_1^{-1}\widetilde{\boldsymbol{\theta}}_1 + \widetilde{\boldsymbol{\theta}}_2^T\boldsymbol{\Gamma}_2^{-1}\widetilde{\boldsymbol{\theta}}_2$, which depend on parameter estimate errors $\widetilde{\boldsymbol{\theta}}_1, \widetilde{\boldsymbol{\theta}}_2$ and diagonal, positive adaptive gain matrixes $\boldsymbol{\Gamma}_1 \in \mathbb{R}^{20\times 20}, \boldsymbol{\Gamma}_2 \in \mathbb{R}^{5\times 5}$.

Evaluating the time derivative of the CLF along the state trajectories (11)–(12) and assuming $-\mathbf{z}_1^T r\mathbf{S}\mathbf{z}_1 = 0$ yields

$$\begin{aligned} \dot{\mathbf{V}}_a &= \mathbf{z}_1^T\dot{\mathbf{z}}_1 + \mathbf{z}_2^T\mathbf{M}\dot{\mathbf{z}}_2 + \dot{\mathbf{V}}_{\mathrm{phi}} \\ &= \mathbf{z}_1^T\left[\boldsymbol{\alpha} - \mathbf{J}^T(\boldsymbol{\eta})\dot{\boldsymbol{\eta}}_{\mathrm{d}}\right] \\ &\quad + \mathbf{z}_2^T\left[\mathbf{z}_1 + \boldsymbol{\theta}\widehat{\mathbf{u}} + \boldsymbol{\varphi}_1^T\widehat{\boldsymbol{\theta}}_1 + \boldsymbol{\varphi}_2^T\widehat{\boldsymbol{\theta}}_2\right] \\ &\quad + \mathbf{z}_2^T\left[\boldsymbol{\varphi}_1^T\widetilde{\boldsymbol{\theta}}_1 + \boldsymbol{\varphi}_2^T\widetilde{\boldsymbol{\theta}}_2\right] + \dot{\mathbf{V}}_{\mathrm{phi}}. \end{aligned} \tag{16}$$

The time derivative

$$\dot{\mathbf{V}}_{\text{phi}} = -\widetilde{\boldsymbol{\theta}}_1^T \boldsymbol{\Gamma}_1{}^{-1} \dot{\widehat{\boldsymbol{\theta}}}_1 - \widetilde{\boldsymbol{\theta}}_2^T \boldsymbol{\Gamma}_2{}^{-1} \dot{\widehat{\boldsymbol{\theta}}}_2 \tag{17}$$

is calculated under the assumption that $\dot{\widetilde{\boldsymbol{\theta}}}_i = -\dot{\widehat{\boldsymbol{\theta}}}_i$ approximately.

Next, grouping (16) yields

$$\begin{aligned} \dot{\mathbf{V}}_a = {} & \mathbf{z}_1^T \left[\boldsymbol{\alpha} - \mathbf{J}^T(\boldsymbol{\eta})\, \dot{\boldsymbol{\eta}}_{\mathrm{d}}\right] \\ & + \mathbf{z}_2^{\mathrm{T}} \left[\mathbf{z}_1 + \boldsymbol{\theta}\hat{\mathbf{u}} + \boldsymbol{\varphi}_1^T \widehat{\boldsymbol{\theta}}_1 + \boldsymbol{\varphi}_2^T \widehat{\boldsymbol{\theta}}_2\right] \\ & + \widetilde{\boldsymbol{\theta}}_1^T \left(\boldsymbol{\varphi}_1 \mathbf{z}_2 - \boldsymbol{\Gamma}_1{}^{-1} \dot{\widehat{\boldsymbol{\theta}}}_1\right) + \widetilde{\boldsymbol{\theta}}_2^T \left(\boldsymbol{\varphi}_2 \mathbf{z}_2 - \boldsymbol{\Gamma}_2{}^{-1} \dot{\widehat{\boldsymbol{\theta}}}_2\right). \end{aligned} \tag{18}$$

According to LaSalle's invariance principle, the controls $\boldsymbol{\alpha}$ and $\hat{\mathbf{u}}$ are chosen in such a way as to make the time derivative of the CLF

$$\dot{\mathbf{V}}_a = -\mathbf{z}_1^T \mathbf{K}_1 \mathbf{z}_1 - \mathbf{z}_2^T \mathbf{K}_2 \mathbf{z}_2 \leq 0 \tag{19}$$

negative semidefinite, with control gain matrixes $\mathbf{K}_i \in \mathbb{R}^{3\times 3}$, $i = \{1, 2\}$, diagonal, positive definite.

The process is carried out in several steps.

1. Using (18), the adaptive laws

$$\dot{\widehat{\boldsymbol{\theta}}}_1 = \boldsymbol{\Gamma}_1 \boldsymbol{\varphi}_1 \mathbf{z}_2, \tag{20}$$

$$\dot{\widehat{\boldsymbol{\theta}}}_2 = \boldsymbol{\Gamma}_2 \boldsymbol{\varphi}_2 \mathbf{z}_2 \tag{21}$$

are chosen to enforce closed-loop stability.

2. The stabilizing function vector

$$\boldsymbol{\alpha} = -\mathbf{K}_1 \mathbf{z}_1 + \mathbf{J}^T(\boldsymbol{\eta})\, \dot{\boldsymbol{\eta}}_{\mathrm{d}} \tag{22}$$

and its derivative

$$\begin{aligned} \dot{\boldsymbol{\alpha}} &= [\dot{\alpha}_1, \dot{\alpha}_2, \dot{\alpha}_3]^T \\ &= -\mathbf{K}_1 \dot{\mathbf{z}}_1 - r\mathbf{S}\mathbf{J}^T(\boldsymbol{\eta})\, \dot{\boldsymbol{\eta}}_{\mathrm{d}} + \mathbf{J}^T(\boldsymbol{\eta})\, \ddot{\boldsymbol{\eta}}_{\mathrm{d}} \end{aligned} \tag{23}$$

are taken independently of uncertainties to make the first bracket term in (18) equal to $-\mathbf{K}_1 \mathbf{z}_1$.

3. The vector of controls $\hat{\mathbf{u}}$ is taken to satisfy the equivalence

$$\boldsymbol{\theta}\hat{\mathbf{u}} = -\mathbf{K}_2 \mathbf{z}_2 - \mathbf{z}_1 - \boldsymbol{\varphi}_1^T \widehat{\boldsymbol{\theta}}_1 - \boldsymbol{\varphi}_2^T \widehat{\boldsymbol{\theta}}_2, \tag{24}$$

which results from making the second bracket term in (18) equal to $-\mathbf{K}_2 \mathbf{z}_2$, and as a consequence of correct estimation of uncertainties $\widehat{\boldsymbol{\theta}}_1$, $\widehat{\boldsymbol{\theta}}_2$ by (20) and (21).

A simplified block diagram of the vectorial backstepping controller for the DP ship model is presented in Fig. 3.

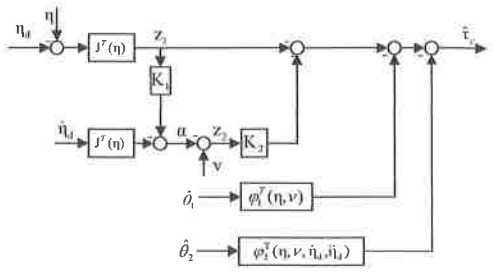

Fig. 3. Simplified diagram of the DP controller.

3.2. Stability analysis. The theoretical analysis of system stability is based on Lyapunov theory and the following lemmas.

Lemma 1. (Lyapunov) *Assume that a scalar function $V(t,x) : \mathbb{R} \to \mathbb{R}$ can be found such that*

1. *$V(t,x)$ is lower bounded,*
2. *$\dot{V}(t,x)$ is negative semidefinite along the trajectories of $\dot{x}$,*
3. *$\dot{V}(t,x)$ is uniformly continuous in time.*

Then $\dot{V}(t,x) \to 0$ as $t \to \infty$.

Lemma 2. (Barbalat) *If $\ddot{V}(t)$ is bounded, then $\dot{V}(t)$ is uniformly continuous in time.*

The stability of the equilibrium point $[\mathbf{z}_1, \mathbf{z}_2] = 0$ is established by using Assumption 2 and based on Lemmas 1 and 2 (Krstić *et al.*, 1995). In fact, due to (20)–(21) the CLF derivative $\dot{\mathbf{V}}_a$ is negative semidefinite (19). This implies that the signals $\mathbf{z}_1, \mathbf{z}_2$ and $\widetilde{\boldsymbol{\theta}}_1, \widetilde{\boldsymbol{\theta}}_2$ are uniformly bounded. Consequently, $\widehat{\boldsymbol{\theta}}_2, \widehat{\boldsymbol{\theta}}_1$ have also the same property, because of slowly varying $\boldsymbol{\theta}_2, \boldsymbol{\theta}_1$. The latter results from Assumption 2.3 and (8)–(9), which implies that the system states $\boldsymbol{\eta}, \boldsymbol{\alpha}, \mathbf{v}$ as well the control $\hat{\mathbf{u}}$ in (24) are uniformly bounded. Therefore, all signals in the closed-loop control system are globally uniformly ultimately bounded. Consequently, the signals $\dot{\boldsymbol{\eta}}, \dot{\boldsymbol{\alpha}}$, and $\dot{\mathbf{v}}$ are bounded, and then also $\dot{\mathbf{z}}_1, \dot{\mathbf{z}}_2$ are bounded. That implies the boundedness of $\ddot{\mathbf{V}}_a(t)$. According to Lemma 2, the CLF derivative is a uniformly continuous function of time. Finally, since $\mathbf{V}_a$ is lower bounded, from Lemma 1 it is concluded that $\dot{\mathbf{V}}_a \to 0$ as t tends to infinity, so the tracking errors $\|\mathbf{z}_1\|$ and $\|\mathbf{z}_2\|$ tend to zero asymptotically as t goes to infinity.

4. Formulating the control allocation task

Based on the backstepping control law (24), the system of linear equations

$$\boldsymbol{\theta}\hat{\mathbf{u}} = \hat{\boldsymbol{\tau}}_c, \tag{25}$$

where

$$\widehat{\tau}_c = -\mathbf{K}_2\mathbf{z}_2 - \mathbf{z}_1 - \boldsymbol{\varphi}_1^T\widehat{\boldsymbol{\theta}}_1 - \boldsymbol{\varphi}_2^T\widehat{\boldsymbol{\theta}}_2, \tag{26}$$

is to be solved to obtain the commanded actuator settings $\widehat{\mathbf{u}}$. This is executed by the CA algorithm. The vector $\widehat{\tau}_c \in \mathbb{R}^{3\times 1}$ (26) gives the virtual control input to the CA algorithm. The CA unit distributes the input $\widehat{\tau}_c$ among the thrusters $\widehat{\mathbf{u}} \in \mathbb{R}^{\mathrm{r}\times 1}$ installed on the vessel. It incorporates lower and upper actuator positions and maximal individual actuator rate constraints,

$$\mathbf{u}_{\min} \le \widehat{\mathbf{u}} \le \mathbf{u}_{\max},$$
$$\dot{\mathbf{u}}_{\min} \le \dot{\widehat{\mathbf{u}}} \le \dot{\mathbf{u}}_{\max},$$

while minimizing the energy consumption of actuators.

The control allocation task can be formulated as the quadratic programming optimization problem

$$\boldsymbol{\Omega}: \min_{\mathbf{u}_{\min}\le\widehat{\mathbf{u}}\le\mathbf{u}_{\max}} \|\boldsymbol{\theta}\widehat{\mathbf{u}} - \widehat{\tau}_c\|_2, \tag{27}$$

$$\widehat{\mathbf{u}}: \min_{\widehat{\mathbf{u}}\in\boldsymbol{\Omega}} \|\mathbf{W}\widehat{\mathbf{u}}\|_2, \tag{28}$$

and solved using various methods. According to Assumption 1.4 and neglecting actuator constraints, the control allocation law

$$\widehat{\mathbf{u}} = \boldsymbol{\theta}^+\left(-\mathbf{K}_2\mathbf{z}_2 - \mathbf{z}_1 - \boldsymbol{\varphi}_1^T\widehat{\boldsymbol{\theta}}_1 - \boldsymbol{\varphi}_2^T\widehat{\boldsymbol{\theta}}_2\right) \tag{29}$$

for the system (25) can be computed by using

$$\boldsymbol{\theta}^+ = \boldsymbol{\theta}^T\left(\boldsymbol{\theta}\boldsymbol{\theta}^T\right)^{-1}, \tag{30}$$

called the Moore–Penrose pseudoinverse matrix.

For a ship with a redundant set of actuators and actuator constraints, the problem of control allocation (27), (28) can be solved numerically.

A number of numerical methods were used in simulations to find the best force distribution. For the general case, the sequential least squares (SLS) method solves the CA problem in two phases. In the first one, the set $\boldsymbol{\Omega}$ of feasible control inputs $\widehat{\mathbf{u}} \in \mathbb{R}^{\mathrm{r}\times 1}$ that minimize the criterion of Eqn. (27) with respect to (27) is given. In the second phase, the optimal control input $\widehat{\mathbf{u}}$ is picked from $\boldsymbol{\Omega}$ to minimize the energy consumption, represented by the square norm of control inputs (28), weighted by $\mathbf{W} \in \mathbb{R}^{\mathrm{r}\times\mathrm{r}}$. The minimal least squares (MLSs) method is a special case of the SLS method which uses active set methods to pick a minimal length solution (28) when (27) does not have a unique feasible solution. The cascaded generalised inverse (CGI) method suggests computing the pseudoinverse solution (30) iteratively. When analyzing a single method step, it is assumed that all pseudoinverse solutions which violate the constraints are saturated and removed from the optimization process. Then the control allocation problem is resolved only for the remaining so-called free control variables, by finding a new pseudoinverse solution. Saturated variables are neglected by removing relevant elements from matrix $\mathbf{K}$. The algorithm is repeated until all control inputs are saturated, or all pseudoinverse solutions meet the constraints.

All CA algorithms considered are described in detail by Harkegard (2004).

5. Simulation results and performance evaluation

The correctness and quality of the designed adaptive dynamic position control system with control allocation were checked on a control system for which the general scheme is shown in Fig. 4. The system includes mathematical models of the kinematics (1) and the dynamics (2) of the ship as a steering object, complemented by the equations of low frequency wave disturbances (3), the actuator dynamics (5) and the thruster model (4). The system also comprises second-order low-pass filter (32), the adaptive dynamic positioning control law (24) and the control allocation algorithm (27)–(28). The values of parameters $\boldsymbol{\theta}_1$ and $\boldsymbol{\theta}_2$ were estimated using the adaptive backstepping method according to the rule (20)–(21).

Considering the mathematical ship model with mass $m = 4,591 \cdot 10^6\,\mathrm{kg}$ and length $L = 76.2\,\mathrm{m}$, the dimensionless matrices of the over-actuated system are given by

$$\begin{aligned}
\mathbf{D}'' &= [(0.0358 + 1.3\,|u''|)\;0\;0;\\
&\quad 0\;(0.1183 + 25\,|v''|)(-0.0138 - 10\,|r''|);\\
&\quad 0\;(-0.0138 - 10\,|v''|)(0.0304 + 5\,|r''|)],\\
\mathbf{M}'' &= [1.1274\;0\;0;\\
&\quad 0\;1.8902\;\;-0.0744; 0\;-0.0744\;0.1278],\\
\mathbf{C}'' &= [0\;0\;(-1.8902v'' + 0.0744r'');\\
&\quad 0\;0\;1.1274u'';\\
&\quad (1.8902v'' - 0.0744r'')\;\;-1.1274u''\;0],
\end{aligned}$$

$$\mathbf{T}'' = 5.0\sqrt{\frac{g}{L}}\mathbf{I}_{6\times 6}.$$

The nonlinear ship model used in the paper is based on the works of Fossen *et al.* (1996) and Godhavn *et al.* (1998). The ship model was identified based on sea trials performed at a constant speed of $U_0 = 0.2\,\mathrm{m/s}$ in calm waters. The vessel is equipped with two main propellers (port and starboard), two aft and one bow tunnel thrusters, and one rotatable bow azimuth thruster. The control variable (propeller revolution vector) consists of six elements $\mathbf{u} = [u_1, u_2, u_3, u_4, u_5, u_6]^T$. The actuator

configuration matrix

$$\mathbf{B}'' = \begin{bmatrix} 1 & 1 & 0 & 0 & 0 & \cos\beta \\ 0 & 0 & 1 & 1 & 1 & \sin\beta \\ l_1 & -l_2 & -l_3 & -l_4 & l_5 & l_6 \sin\beta \end{bmatrix} \quad (31)$$

depends on the moment arms given by the locations of actuators $l_i, i \in \{1, \ldots, 6\}$ and the azimuth angle β. The non-dimensional system matrices

$$\begin{aligned} \mathbf{B}'' = [&1\ 1\ 0\ 0\ 0\ 0; \\ &0\ 0\ 1\ 1\ 1\ 1; \\ &0.0472 - 0.0472\ -0.4108 \\ &-0.3858\ 0.4554\ 0.3373], \\ \mathbf{K}'' = 10^{-3}&\mathrm{diag}([9.3\ 9.3\ 2.0\ 2.0\ 2.8\ 2.6]), \end{aligned}$$

in the vessel model considered are given for $\beta = 90^0$. These values were normalized in accordance to the "Bis-system", where the thruster inputs $u_i'', i \in \{1, \ldots, 6\}$ were scaled to $[-1, 1]$. The following scaling factors:

$$\mathbf{T} = \sqrt{\tfrac{L}{g}}\mathbf{I}_{6\times 6}\mathbf{T}'', \quad \boldsymbol{\eta} = \mathrm{diag}\left([L, L, 1]\right)\boldsymbol{\eta}'',$$
$$\mathbf{v} = \mathrm{diag}\left(\left[\sqrt{gL}, \sqrt{gL}, \sqrt{\tfrac{g}{L}}\right]\right)\mathbf{v}''$$

were used to calculate dimensional states and time constants with $g = 9.81\,\mathrm{m/s^2}$. The actuator time constants were chosen equal to 5 s for all thrusters and propellers. Moreover, the velocity constraints $|u| \leq 4\,\mathrm{m/s}$, $|v| \leq 1\,\mathrm{m/s}$, $|r| \leq 1\,\mathrm{deg/s}$ were considered for the dimensional model.

Smooth, bounded reference trajectories $\boldsymbol{\eta}_\mathrm{d}$ and their first-and second-order derivatives $\dot{\boldsymbol{\eta}}_\mathrm{d}, \ddot{\boldsymbol{\eta}}_\mathrm{d}$ were generated by using the 2nd-order low-pass filter

$$G_f(\mathrm{s}) = \frac{\omega_n^2}{\mathrm{s}^2 + 2\zeta\omega_n\mathrm{s} + \omega_n^2}, \quad (32)$$

with relative damping ratios equal to $\zeta = 1$ and natural frequencies equal to $\omega_n = 0.1\,\mathrm{rad/s}$.

5.1. Simulation tests. This section describes numerical simulation tests performed to verify the performance of the proposed DP adaptive control law with control allocation. The tests included programmed inertial changes of the set position and heading in the presence of slowly varying disturbances. The backstepping control law was numerically simulated with the dimensionless sampling time $h = 0.1$ and the Euler-method based numerical integration procedure. In Test 1, the design parameters of the adaptive output feedback controller were determined and the properties of CA algorithms were compared. In Test 2, system sensitivity to changes in model parameters was studied after introducing the parameter projection operator to the adaptive law (El Maguiri *et al.*, 2010; Krstić *et al.*, 1995).

5.1.1. Test 1. At the beginning, the least squares method and a genetic algorithm were applied to choose the numeric values of the control gain matrices $\mathbf{K}_1 = \mathrm{diag}(0.1, 0.1, 0.1)$, $\mathbf{K}_2 = \mathrm{diag}(5, 5, 3)$. Also, the particle swarm optimization (PSO) algorithm was used to tune the adaptive gain matrices,

$$\begin{aligned} \boldsymbol{\Gamma}_1 = \mathrm{diag}(&300\ 747\ 10\ 10\ 299\ 4.13 \cdot 10^6 \\ &6.16 \cdot 10^7\ 0\ 0\ 1 \cdot 10^5\ 1 \cdot 10^5\ 0\ 0\ 1.44 \cdot 10^7 \\ &1.71 \cdot 10^6\ 1 \cdot 10^4\ 1 \cdot 10^5\ 0.002\ 0.002\ 0.002), \\ \boldsymbol{\Gamma}_2 = \mathrm{diag}(&1 \cdot 10^5\ 1.19 \cdot 10^5\ 4.2\ 48\ 7.2 \cdot 10^4). \end{aligned}$$

During the tuning process, typical maneuvering tests were performed with the model described in "Bis-system", to assess the stability and performance of the control algorithm. With zero initial states $\boldsymbol{\eta}(0) = (0,\ 0,\ 0)$, the set values of the position and heading were changed to $(10\,\mathrm{m}, 10\,\mathrm{m}, 10\,\mathrm{deg})$ and maintained until the vessel reached those. Then the set values were changed to $(0\,\mathrm{m}, 0\,\mathrm{m}, 0\,\mathrm{deg})$ and maintained again until the vessel turned with respect to the initial values and started to follow the reference trajectory (32). The system was excited independently in 3 DOFs. The simulation results are depicted in Figs. 5–11. The control gain matrices $\mathbf{K}_1$, $\mathbf{K}_2$ were set based on experimental tests performed, after assuming real values of the estimated parameters, to minimize the control error as the main objective:

$$J_c(t) = \int_0^T \|\boldsymbol{\eta} - \boldsymbol{\eta}_d\|_2^2\ \mathrm{d}t. \quad (33)$$

For tuning $\boldsymbol{\Gamma}_1$, $\boldsymbol{\Gamma}_2$, the search space will be 21-dimensional, with the number of dimensions being the number of non-zero estimated ship model parameters. During the optimization process the initial values of the estimated parameters were equal to 60% of their true values, and the reference signals were excited in the adaptive control framework. The objective was to minimize the fitness function

$$J_a(t) = \int_0^T \left(\left\|\widetilde{\boldsymbol{\theta}}_1\right\|_2^2 + \left\|\widetilde{\boldsymbol{\theta}}_2\right\|_2^2\right)\mathrm{d}t, \quad (34)$$

being the integral square error (ISE) between true values and their estimates. The PSO algorithm runs for the swarm size of 50 until the stop condition is satisfied (function tolerance = $1.0000e-06$ and maximum iterations = 300). The best particle position yields optimized parameters. In the simulations, this method was consequently incorporated to ensure that the norm of estimate errors is minimized and the output tracking error converges to zero. It was demonstrated that the proposed scheme is effective, although it does not ensure the convergence of all parameters to their real

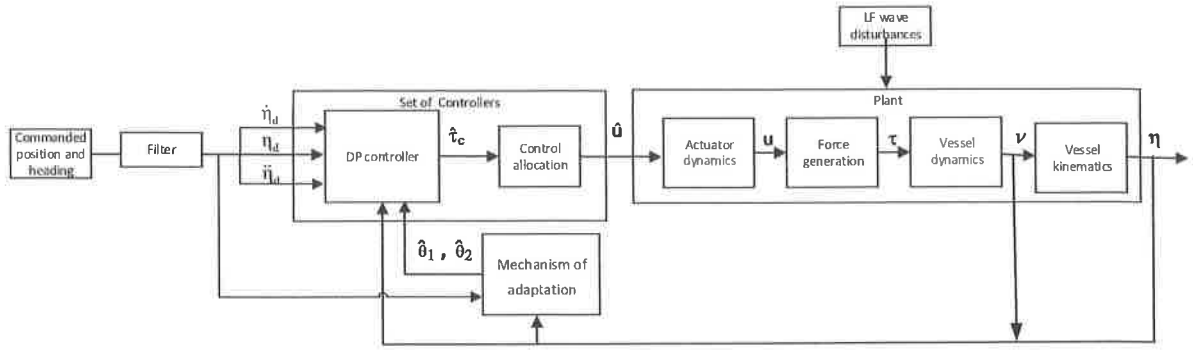

Fig. 4. Simplified diagram of an adaptive DP control structure with control allocation.

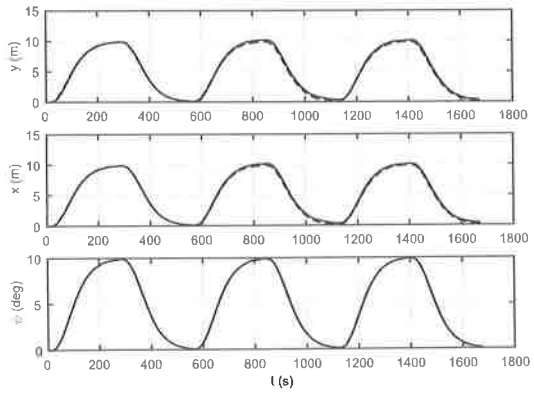

Fig. 5. Actual (η: solid line) and desired (η_d: dotted line) ship position and heading.

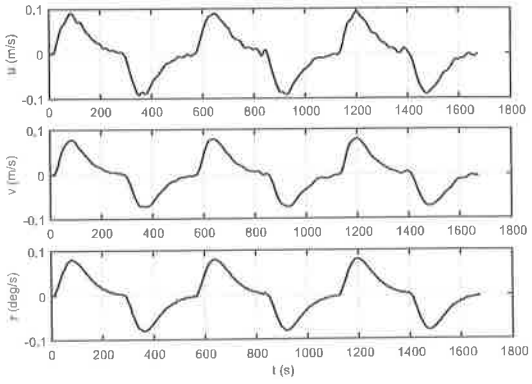

Fig. 6. Ship velocities in surge (u), sway (v) and yaw rate (r).

values. Nevertheless, it guarantees limited changes of all parameters and satisfactory control accuracy (Figs. 5–11).

Secondly, the control allocation-based optimization procedure (27), (28) with the identity matrix $\mathbf{W} = \text{diag}(1,1,1,1,1,1)$ was used for actuator-force mapping. Detailed comparisons were made between the CGI, WLS and MLS algorithms to find the best distribution of commands into individual actuators. The performance indices of the proposed CA algorithm are summarized in Table 1. It contains time quality factors such as maximum and mean computational time, the normalized quality factors, the minimum norm of the control allocator (27) and the minimum norm of the actuator activities (28). The simulations were performed on an Intel Core i73612QM CPU 2.10 GHz computer. The mean and max computation times shown in Table 1 were averaged over 30 runs. The remaining factors, including the normalized norm of control errors for x, y and ψ, correspond to the best solution of CA and were scaled by the number of sampling times during the simulation. As can be seen in Table 1, the control allocation objective is satisfied, giving suboptimal results due to actuator constraints. The quality factors of MLS and CGI differ only by computation time and are much better than those of the WLS algorithm. The best computation time is obtained for the CGI algorithm.

Figures 5–11 present the tracking performance of the adaptive DP control law, with the initial vector of the estimated parameters assumed equal to 60% of the corresponding true values. The presented results confirm good performance of the proposed control system in the presence of unknown slowly varying model parameters and disturbance uncertainties. It can be clearly observed in Figs. 5–7 and Table 1 that the proposed algorithm asymptotically adjusts the position and heading to the desired values. The control errors tend to zero without oscillations in the surge, sway and yaw directions. When analyzing the optimization process in Fig. 8, we can see that the command control forces $\widehat{\tau}_c$ calculated from

Table 1. Quality factors of CA algorithms.

CA	t_{max}(ms)	t_{mean}(ms)	$\|\boldsymbol{\theta}\widehat{\mathbf{u}} - \widehat{\boldsymbol{\tau}}_c\|_2$	$\|\widehat{\mathbf{u}}\|_2$	$\|e_x\|_2$	$\|e_y\|_2$	$\|e_\psi\|_2$
CGI	1.1747	0.041728	2.6714e-19	6.2437e-04	6.8964e-06	8.0893e-06	5.3454e-04
WLS	11.6087	0.068164	3.2491e-19	6.2436e-04	6.9313e-06	8.7659e-06	6.3858e-04
MLS	8.0324	0.049132	2.6714e-19	6.2437e-04	6.8964e-06	8.0893e-06	5.3454e-04

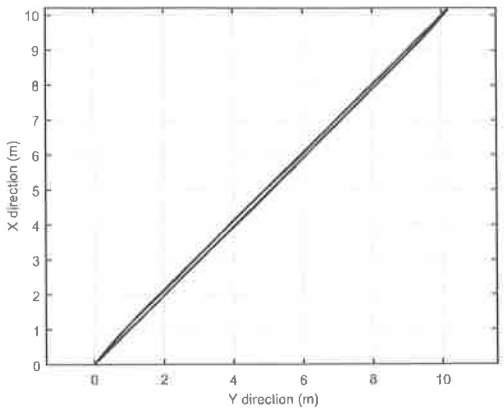

Fig. 7. Resulting ship trajectory.

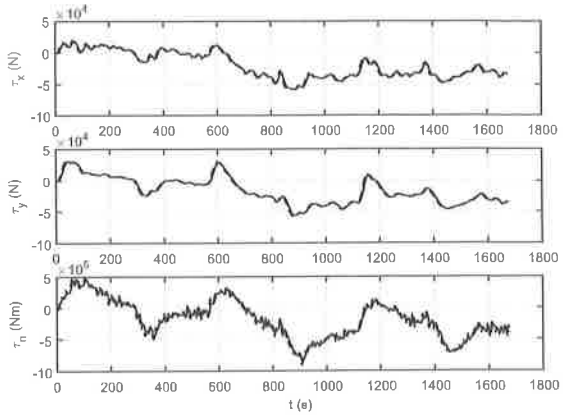

Fig. 8. Command ($\widehat{\boldsymbol{\tau}}_c$: dotted line) control forces and the actual ($\boldsymbol{\tau}$: solid line) control forces generated by the actuators.

the adaptive control law track well the actual forces $\boldsymbol{\tau}$ generated by the ship actuators. The normalized command $\widehat{\mathbf{u}}$ actuator values were calculated from the CGI control allocation algorithm shown in Fig. 11. It can be clearly observed in Figs. 9 and 10 that selected parameters tend to their real values and all of them change in a limited manner. These simulation results illustrate that all numerically correct values for the hydrodynamic parameters are not necessary to achieve accurate tracking.

5.1.2. Test 2. The vessel continues the maneuver from Test 1 and after $t_1 = 1672.8\,\mathrm{s}$ moves towards the reference point $(10\,\mathrm{m}, 10\,\mathrm{m}, 10\,\mathrm{deg})$. After $t_2 = t_1 + 557.6\,\mathrm{s}$ it changes its reference values and starts to move towards the point $(15, 20, 20)$. Then, after $t_3 = t_2 + 557.6\,\mathrm{s}$ it starts to move towards point $(15, 30, 20)$, keeping constant heading. The simulation tests were performed for different initial values of estimates and different values of model parameters. The results of system sensitivity tests to changes of initial estimate values, within the range of 60% to 90% of real values are given in Figs. 12–15, while those presenting system sensitivity to model parameter changes, also within the 60% to 90% range, are shown in Figs. 16–19. It is noteworthy that the reference inputs for many online applications are event based and not known *a priori*, therefore it is often impossible to monitor online a signal and excite it. Consequently, the convergence of parameters often cannot be guaranteed in practice for many adaptive control applications. For this reason, a projection algorithm has been introduced into the system described earlier. The use of the projection algorithm means that there is no need for online convergence, and hence the need for introducing an excitation signal disappears.

To prevent a possible drift of parameter estimates which may result from state estimation errors, the parameter projection operator (El Maguiri *et al.*, 2010) was introduced to the parameter adaptive laws (20), (21). The proposed operator was used to project the parameter estimate $\widehat{\theta}_i(j)$ onto a bounded convex set including the true parameter $\theta_i(j)$. The convex set can be any interval $|\widehat{\theta}_i(j)| \leq \epsilon_i(j)$ such that $\epsilon_i(j) \geq |\theta_i(j)|$. The value of $\epsilon_i(j)$ was equal to 150% of real parameter value. The initial vector of estimated parameters was assumed equal to 60% of their real values. The obtained values of the estimates change in the assumed limited manner in transient states due to changes in the set values, but in steady states of state variables they are approximately constant (Figs. 14–15, 18–19).

In Fig. 13 can be seen that the command and actual control forces $\widehat{\boldsymbol{\tau}}_c$ and control errors do not depend significantly on changes in initial estimates. However, in Fig. 17 it can be seen that they depend on changes in model parameters. Nevertheless, in Figs. 12–13 and 16–17 it can be clearly observed that the proposed

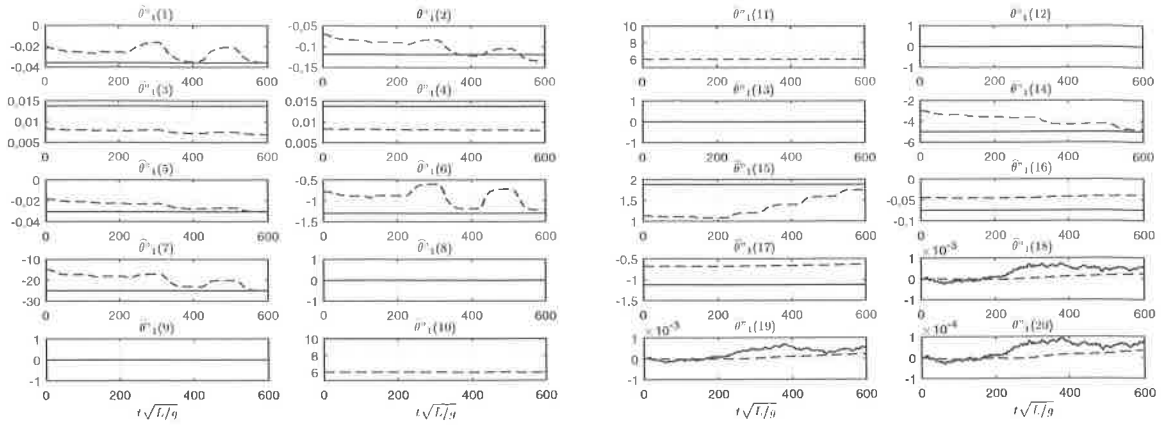

(a) (b)

Fig. 9. Normalized estimates (dotted line) and the actual (solid line) vector $\boldsymbol{\theta}_1$ components: $\boldsymbol{\theta}_1(1:10)$ (a), $\boldsymbol{\theta}_1(11:20)$ (b).

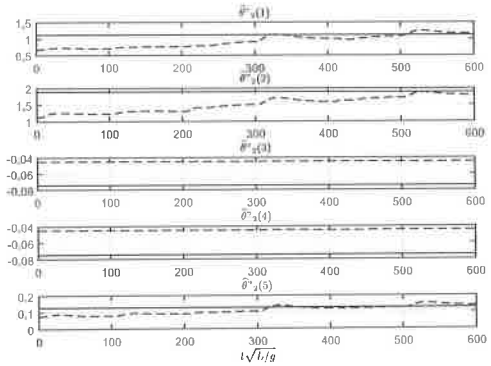

Fig. 10. Normalized estimates (dotted line) and the actual (solid line) vector $\boldsymbol{\theta}_2$ components.

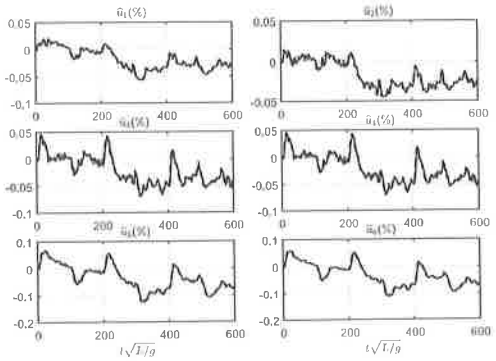

Fig. 11. Normalized command (dotted line) and the actual (solid line) actuator signals ($\widehat{\mathbf{u}}$).

algorithm asymptotically adjusts the position and heading to their desired values. The control errors tend to zero without oscillations in the surge, sway and yaw directions in the presence of uncertainties. Test 2 illustrates that all numerically correct values of all hydrodynamic parameters are not necessary to achieve accurate tracking. This demonstrates the robustness of the proposed DP control system. The simulation results show that the proposed DP adaptive control algorithm is effective and exhibits satisfactory performance in the case of model uncertainties.

6. Conclusions

In the paper, an adaptive backstepping control law with control allocation was developed for a dynamically positioned ship. The control law was designed to compensate ship dynamics model uncertainties and environmental disturbances in the presence of inertia matrix uncertainties. The effectiveness of the proposed method was presented by means of numerical examples and evaluated by tracking its accuracy and robustness for uncertainties with the parameter projection operator. The over-actuated system simulation tests were performed using all available actuators. The forces and torque computed from the adaptive control law were allocated to individual thrusters by employing quadratic programming. The performance assessment of different control allocation algorithms making use of WLS, CGI and MLS was presented.

The comparison between CA algorithms shows that the best optimization performance is obtained by using CGI. Moreover, by combining the proposed dynamic adaptive control law with control allocation it was shown that excellent tracking performance and the ability to compensate for model uncertainties can be achieved even if the operating points are subject to changes. Based on the performed simulation tests, a conclusion can be made that the proposed method achieves acceptable performance in the case of unknown matrices **C**, **D** and **M**. The

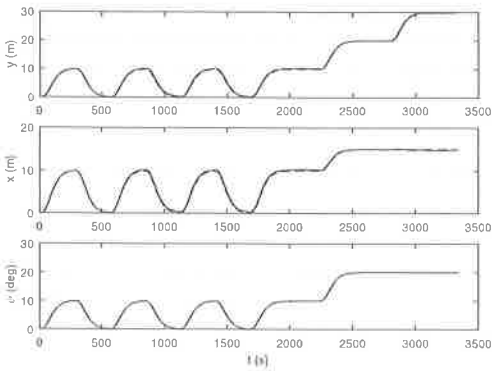

Fig. 12. Actual (η: solid line) and desired (η_d: dotted line) ship position and heading.

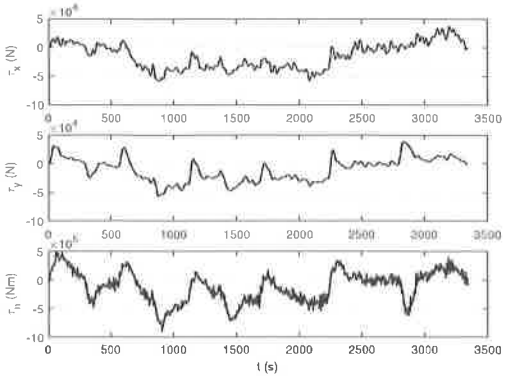

Fig. 13. Command ($\widehat{\tau}_c$: dotted line) control forces and the actual (τ: solid line) control forces generated by the actuators.

proposed design procedure of a DP control system with uncertainties is general and can be applied to other marine vessels, as well as to aircraft or mobile robots which can be represented by a similar state-space model.

The proposed DP control system neglects the actuator dynamics. However, it seems well justified to consider the actuator dynamics in the DPS, as it exerts influence on two main subsystems. Firstly, it can improve the control accuracy of the designed DP control system, and secondly, it can improve control allocation process. These issues will be analyzed as part of future research.

References

Bańka, S., Dworak, P. and Jaroszewski, K. (2013). Linear adaptive structure for control of a nonlinear MIMO dynamic plant, *International Journal of Applied Mathematics and Computer Science* **23**(1): 47–63, DOI: 10.2478/amcs-2013-0005.

Bodson, M. (2002). Evaluation of optimization methods for control allocation, *Journal of Guidance, Control and Dynamics* **25**(4): 703–711.

Boulkroune, A., Bounar, N., M'Saad, M. and Farza, M. (2014). Indirect adaptive fuzzy control scheme based on observer for nonlinear systems: A novel SPR-filter approach, *Neurocomputing* **135**(C): 378–387, DOI: 10.1016/j.neucom.2013.12.011.

Du, J., Hu, X., Liu, H. and Chen, C.L.P. (2015). Adaptive robust output feedback control for a marine dynamic positioning system based on a high-gain observer, *IEEE Transactions on Neural Networks and Learning Systems* **26**(11): 2775–2786.

El Maguiri, O.E., Giri, F., Dugard, L., Fadil, H.E. and Chaoui, F.Z. (2010). Nonlinear adaptive output feedback control of series resonant dc-dc converters, *Proceedings of the American Control Conference, Baltimore, MD, USA*, pp. 3287–3292, DOI: 10.1109/ACC.2010.5530481.

Fossen, T.I. (2000). A survey on nonlinear ship control: From theory to practice, *Proceedings of the 5th IFAC Conference on Manoeuvring and Control of Marine Craft, Aalborg, Denmark*, pp. 1–16.

Fossen, T.I. (2011). *Handbook of Marine Craft Hydrodynamics and Motion Control*, John Wiley and Sons Ltd, Chichester.

Fossen, T.I., Sagatun, S.I. and Sorensen, A.J. (1996). Identification of dynamically positioning ships, *Control Engineering Practice* **4**(3): 369–376, DOI: 10.1016/0967-0661(96)00014-7.

Fu, M., Xu, Y. and Zhou, L. (2016). Bio-inspired trajectory tracking algorithm for dynamic positioning ship with system uncertainties, *Proceedings of the 35th Chinese Control Conference (CCC), Chengdu, China*, pp. 4562–4566, DOI:10.1109/ChiCC.2016.7554061.

Godhavn, J.M., Fossen, T.I. and Berge, S.P. (1998). Nonlinear and adaptive backstepping designs for tracking control of ships, *International Journal of Adaptive Control and Signal Processing Marine Systems Control* **12**(8): 649–670.

Hanger, M., Johansen, T.A., Mykland, G.K. and Skullestad, A. (2011). Dynamic model predictive control allocation using CVXGEN, *Proceedings of the 9th IEEE International Conference on Control and Automation (ICCA), Santiago, Chile*, DOI: 10.1109/ICCA.2011.6137940.

Harkegard, O. (2004). Dynamic control allocation using constrained quadratic programming, *Journal of Guidance, Control and Dynamics* **27**(6): 1028–1034.

Hassani, V., Sorensen, A.J. and Pascoal, A.M. (2012). Robust dynamic positioning of offshore vessels using mixed-μ synthesis. Part II: Simulation and experimental results, *IFAC Workshop on Automatic Control in Offshore Oil and Gas Production, Trondheim, Norway*, pp. 183–188, DOI: 10.3182/20120531-2-NO-4020.00043.

Johansen, T.A. and Fossen, T.I. (2013). Control allocation—a survey, *Automatica* **49**(5): 1087–1103.

Katebi, M.R., Grimble, M.J. and Zhang, Y. (1997). H/∞ robust control design for dynamic ship positioning, *IEE Proceedings: Control Theory and Applications* **144**(2): 110–120, DOI:10.1049/ip-cta:19971030.

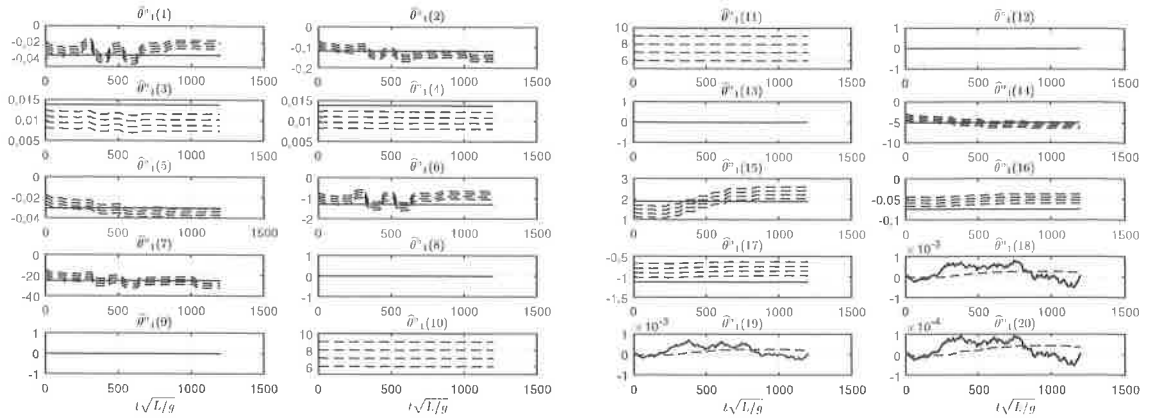

(a) (b)

Fig. 14. Normalized estimates (dotted line) and actual (solid line) vector $\boldsymbol{\theta}_1$ components: $\boldsymbol{\theta}_1(1:10)$ (a), $\boldsymbol{\theta}_1(11:20)$ (b).

Krstić, M., Kanellakopoulos, I. and Kokotović, P. (1995). *Nonlinear and Adaptive Control Design*, Wiley, New York, NY.

Lin, X., Xie, Y., Bian, X. and Zhao, D. (2013). Dynamic positioning controller based on unified model in extreme seas, *Journal of Computational Information Systems* **9**(20): 8089–8097.

Lindegaard, K.P. and Fossen, T.I. (2003). Fuel-efficient rudder and propeller control allocation for marine craft: Experiments with a model ship, *IEEE Transactions on Control Systems Technology* **11**(6): 850–862, DOI:10.1109/TCST.2003.815613.

Loria, A., Fossen, T.I. and Panteley, E. (2000). A separation principle for dynamic positioning of ships: Theoretical and experimental results, *IEEE Transactions on Control Systems Technology* **8**(2): 332–343.

Luo, A., Serrani, A., Yurkovich, S., Doman, D.B. and Oppenheimer, M. W. (2004). Model predictive dynamic control allocation with actuator dynamic, *Proceedings of the 2004 American Control Conference, Boston, MA, USA*, Vol. 2, pp. 1695–1700.

McGookin, E.W., Murray-Smith, D.J., Li, Y. and Fossen, T.I. (2000). Ship steering control system optimisation using genetic algorithms, *Control Engineering Practice* **8**(4): 429–443, DOI: 10.1016/S0967-0661(99)00159-8.

Oppenheimer, M.W., Doman, D.B. and Bolender, M.A. (2006). Control allocation for over-actuated systems, *Proceedings of 14th Mediterranean Conference on Control and Automation, Ancona, Italy*, pp. 1–6, DOI:10.1109/MED.2006.328750.

Sorensen, A.J. (2011). A survey of dynamic positioning control systems, *Annual Reviews in Control* **35**(1): 123–136.

Swaroop, D., Hedrick, J.K., Yip, P.P. and Gerdes, J.C. (2000). Dynamic surface control for a class of nonlinear systems, *IEEE Transactions on Automatic Control* **45**(10): 1893–1899, DOI: 10.1109/TAC.2000.880994.

Tannuri, E.A., Agostinho, A.C., Morishita, H.M. and Moratelli, L. (2010). Dynamic positioning systems: An experimental analysis of sliding mode control, *Control Engineering Practice* **18**(10): 1121–1132, DOI:10.1016/j.conengprac.2010.06.07.

Tomera, M. (2017). Hybrid switching controller design for the maneuvering and transit of a training ship, *International Journal of Applied Mathematics and Computer Science* **27**(1): 63–77, DOI: 10.1515/amcs-2017-0005.

Tsopelakos, A. and Papadopoulos, E. (2017). Design and evaluation of dynamic positioning controllers with parasitic thrust reduction for an overactuated floating platform, *IEEE Transaction on Control Systems and Technology* **25**(1): 145–160.

Witkowska, A. (2013). Dynamic positioning system with vectorial backstepping controller, *Proceedings of the 18th International Conference on Methods and Models in Automation and Robotics (MMAR), Międzyzdroje, Poland*, pp. 842–847.

Witkowska, A. and Śmierzchalski, R. (2012). Designing a ship course controller by applying the adaptive backstepping method, *International Journal of Applied Mathematics and Computer Science* **22**(4): 985–997, DOI: 10.2478/v10006-012-0073-y.

Witkowska, A. and Śmierzchalski, R. (2018). Adaptive dynamic control allocation for dynamic positioning of marine vessel based on backstepping method and sequential quadratic programming, *Ocean Engineering* **163**(1): 570–582.

Xia, G., Xue, J., Jiao, J., Wang, H. and Zhou, H. (2016). Adaptive fuzzy control for dynamic positioning ships with time-delay of actuator, *Proceedings of the MTS/IEEE International Conference on OCEANS, Monterey, CA, USA*, pp. 1–6, DOI:10.1109/OCEANS.2016.7761043.

Zhang, C.-D., Wang, X.-H. and Xiao, J.-M. (2013). Ship dynamic positioning system based on backstepping control, *Journal of Theoretical and Applied Information Technology* **51**(1): 129–136.

Zwierzewicz, Z. (2010). Nonlinear adaptive tracking-control synthesis for functionally uncertain systems, *International Journal of Adaptive Control and Signal Processing* **24**(2): 96–105, DOI: 10.1002/acs.1114.

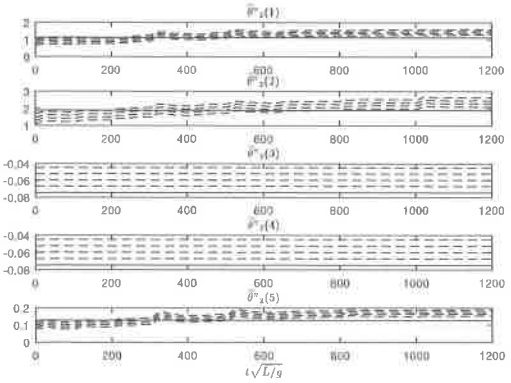

Fig. 15. Normalized estimates (dotted line) and the actual (solid line) vector $\boldsymbol{\theta}_2$ components.

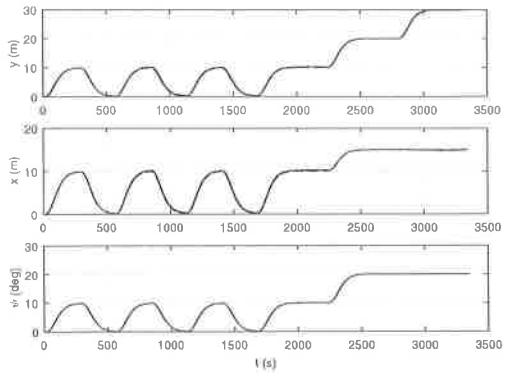

Fig. 16. Actual ($\boldsymbol{\eta}$: solid line) and desired ($\boldsymbol{\eta}_{\mathrm{d}}$: dotted line) ship position and heading.

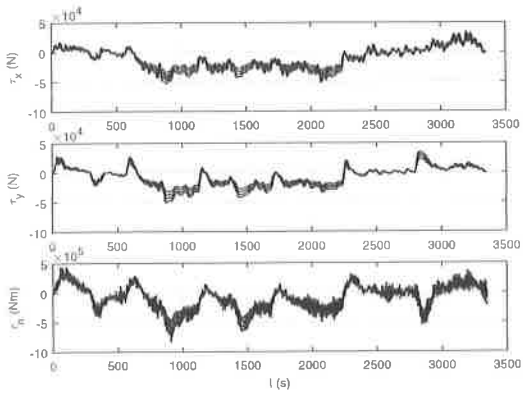

Fig. 17. Command ($\widehat{\boldsymbol{\tau}}_c$: dotted line) control forces and the actual ($\boldsymbol{\tau}$: solid line) control forces generated by the actuators.

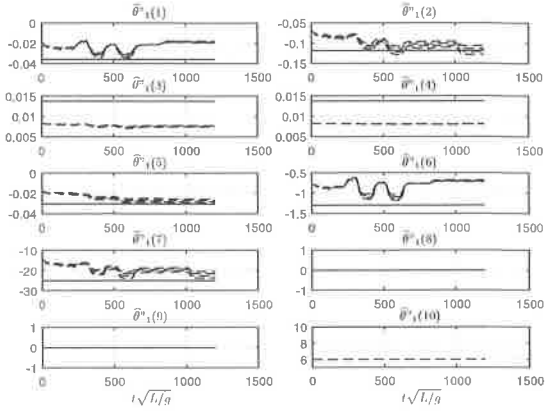

(a)

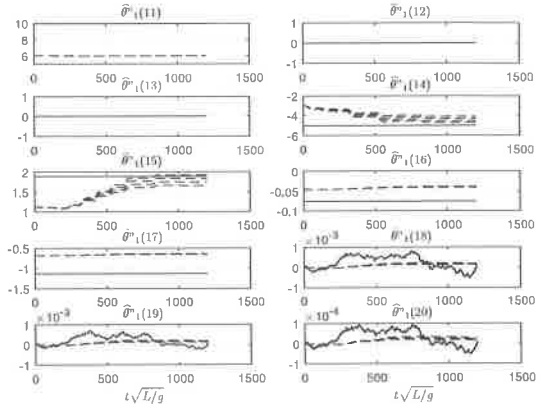

(b)

Fig. 18. Normalized estimates (dotted line) and the actual (solid line) vector $\boldsymbol{\theta}_1$ components: $\boldsymbol{\theta}_1(1:10)$ (a), $\boldsymbol{\theta}_1(11:20)$ (b).

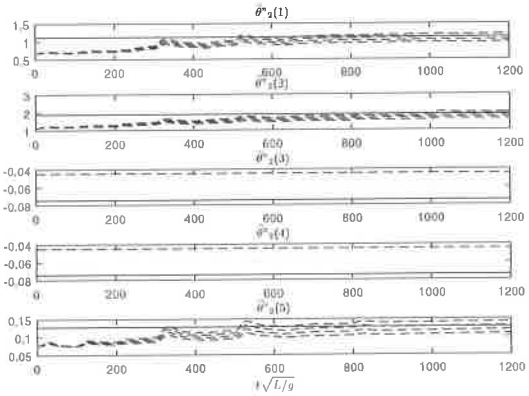

Fig. 19. Normalized estimates (dotted line) and the actual (solid line) vector $\boldsymbol{\theta}_2$ components.

Anna Witkowska holds an from MSc in mathematics and computer science from the University of Gdańsk, Poland (2001), and a PhD in automatic control and robotics (2011) from the Technical University of Warsaw. Currently she is an assistant professor at the Gdańsk University of Technology, Faculty of Electrical and Control Engineering. Her research interests include automation, especially nonlinear control of ocean vehicles.

Roman Śmierzchalski graduated in 1979 from the Technical University of Gdańsk in Poland, Electrical Department, specializing in ship automatics. He received the PhD degree from the Technical University of Gdańsk, Shipbuilding Institute, in 1988, and the DSc degree in automation and robotics from the Technical University of Warsaw, Faculty of Electronic Engineering, in 1999. Currently he is a full professor at the Gdańsk University of Technology, Faculty of Electrical and Control Engineering. He specializes in the development of computer methods of safe control of ship motion. He has published about 150 papers in refereed journal and conference. His current research interests are in the field of artificial intelligent in ship control and automation.

Received: 6 November 2017
Revised: 19 April 2018
Re-revised: 17 August 2018
Accepted: 20 September 2018